Chapter 4. Damage Detection from the Space

After an earthquake occurs, it is vital to identify hard-hit areas and evaluate the degree of damage. The evaluation can be carried out through a field reconnaissance survey. However, it is time consuming and requires a lot of resources. In case of a large natural disaster, a fast assessment of the damaged areas is required to dispatch rescue teams to the heavily damaged areas and draw recovery plans. Satellite remote sensing, which can monitor a large area, may provide effective information on determining damage distribution for recovery activities and restoration planning. The several researchers have already reported spectral characteristics of the damaged area by comparing satellite optical images with the damage survey results on the 1995 Hyogoken-Nanbu (Kobe) earthquake, and have attempted to identify the damage distribution (e.g., Matsuoka and Yamazaki, 1998).

Synthetic aperture radar (SAR) recently became an important sensor of satellite remote sensing. SAR observations can be performed in both day and night time without influence of weather condition. This feature can be useful for effective post-disaster damage assessment, especially when optical remote sensing or a field survey for a large area is difficult. Several researchers reported the interpretation of the building damage distribution using SAR amplitude information (Aoki *et al*., 1998; Yonezawa and Takeuchi, 1998) and phase information (Yonezawa and Takeuchi, 1999; Matsuoka and Yamazaki, 2000a). Using the phase approach, which has higher sensitivity than the intensity approach, crustal deformation due to seismic events was successfully identified (Rosen *et al*., 1999).

In this chapter, in order to identify the different kinds of damage, the comparison of satellite images taken before and after the 1999 Kocaeli, Turkey earthquake is conducted. The optical images from Landsat/TM are used to detect the fire outbreak, the ground subsidence and the building damage (Estrada *et al.*, 2000). The SAR images from ERS are also employed to investigate the backscattering characteristics for the damaged areas due to this earthquake (Matsuoka and Yamazaki, 2000b). These pre- and post-event images are compared to extract damage distributions, and the results were then compared with field survey results.

4.1 Recognition of Damaged Areas Using Optical Images

4.1.1 Satellite Data and Image Registration

The data used in this investigation are remote sensing images from Landsat/TM (TM stands for Thematic Mapper) taken over the affected area. The images were taken on March 27th, 1999, for a pre-event image, and on August 18th, 1999, for a post-event image, it is one day after the event. The images cover an area of 185km x 154km. From these raw images we have selected an area including Golcuk and Adapazari. The reason of the selection of this area is that it was heavily damaged and includes different types of damages (e.g., subsidence, fire, building collapse). Other reason was to reduce the time of computation.

Since the images were acquired at different dates they do not match. In order to compare a pixel-to-pixel comparison, the pixels in the pre- and post-event images should represent the same area on the earth surface. To match two or more images they have to be registered, that is they must be expressed in terms of the same coordinate system. To match two images they can be transformed so that they have the same scale and projection properties on a map, this is called geometric correction. But it needs a geographically correct map and each image has to be corrected separately. A related technique, to match two remote sensed images, called registration, is the fitting of the coordinates of one image to that of a second image of the same area. To make an image-to-image registration one of them is chosen as a master to which the other, known as the slave, is to be registered. In this study the master image is the pre-event image to which the post-event image is registered. The image registration was made using the raw images as shown in Figure 4.1.1, and in the area of 185km x 154km, 250 ground control points were defined. As ground control points well-defined shapes were selected,

like road intersections, border of dams, distinctive water bodies, rivers, etc. Finally, the rotation scaling and translation method was used for warping the slave image and the nearest-neighbor method was used for re-sampling.

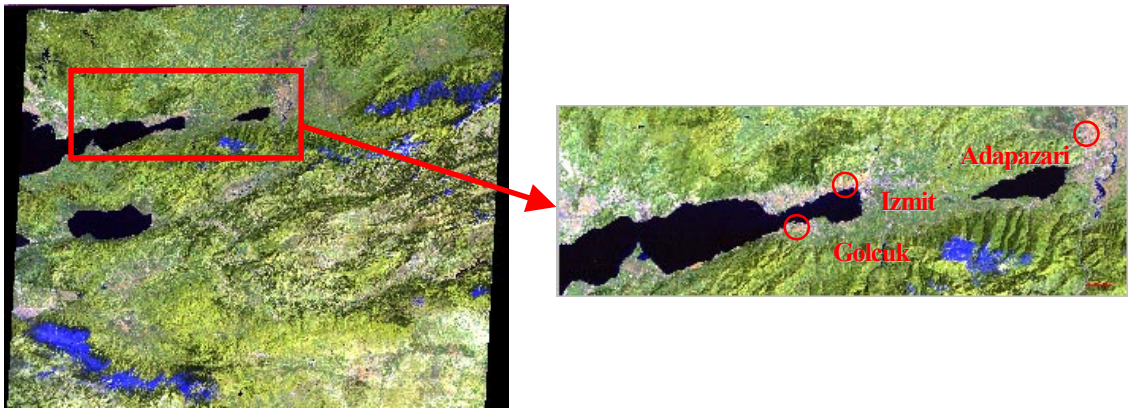

Figure 4.1.1. Raw image taken before the event and selected area of Landsat/TM.

4.1.2 Areas Damaged by Fire

The Tupras refinery, located in Korfez, suffered a very large damaged due to the fire ignited in the naphtha tank after the shake and spread into the tank farm by combustible spill (MCEER, 2000). The fire as well as the heat caused damage to numerous tanks and due to breaks in the pipelines, the refinery lost fire-fighting capability and it took several days to have the fire under control. To identify the areas affected by fire through remote sensing data we compare the profiles of the pre- and post-event images. The profile represents the distribution of the digital number (*DN*) of certain band along a strip of the image (*DN* represents the level of reflectance of certain ground area). This strip can be taken over the X-axis or Y-axis. For this comparison the band 6 (far infrared band) is used. Before making the comparison, the correction for seasonal effect is made. This correction was made by subtracting the average difference between the digital numbers of the images (pre- and post-event) from the values of the digital number of the post-event image.

We can see in Figure 4.1.2 that there is a pattern in the profile before the earthquake as well as in the after one. But in the region between sample 100 and sample 200, in the X-axis, and between the line 500 and 600, in the Y-

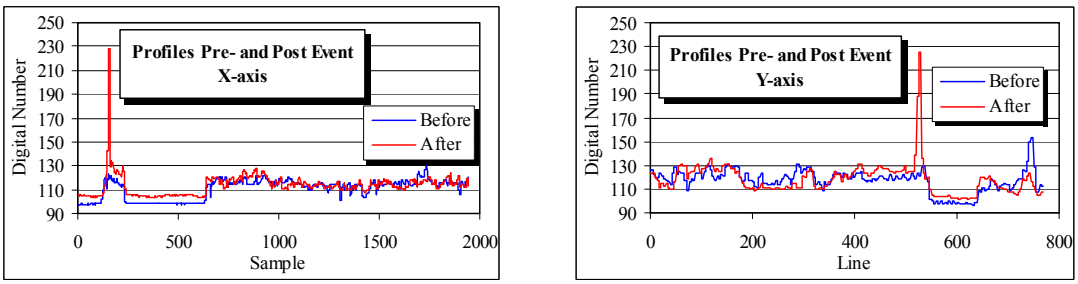

(a) (b)

Figure 4.1.2. Profile of the pre- and post-event images of the band 6: (a) Profile along the X-axis; and (b) Profile along the Y-axis. Notice the peak value represents the area around Tupras Refinery.

axis (this section corresponds to the refinery), there is a peak value in the post-event profile that identifies the high temperature due to the fire outbreak at the refinery. The flat pattern sections in this graph represent the area of the sea and the section with small changes in *DN* belongs to the ground surface. The composite RGB images are shown in Figure 4.1.3.

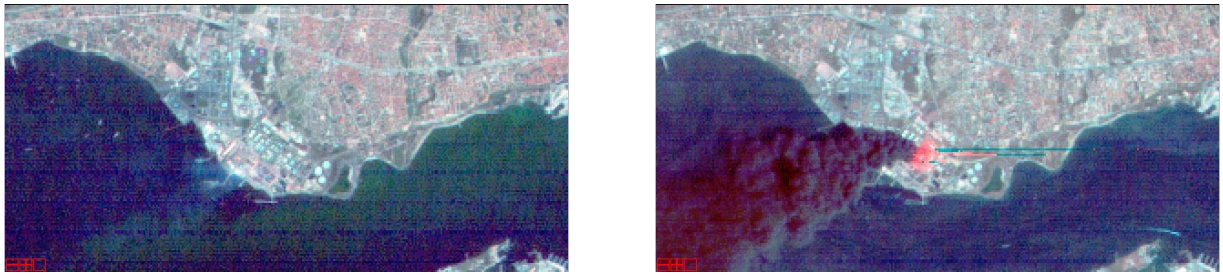

(a) (b)

Figure 4.1.3. Images (RGB 721) around Tupras Refinery: before (a) and after (b) earthquake images, respectively. In Fig. (b), the fume coming up from the refinery and the fire can be noticed (Refer to color Figure 6).

4.1.3 Subsidence

A huge scale ground subsidence occurred at Golcuk. The ground subsidence took as a result of normal faulting associated with the main lateral strike slip event (Aydan *et al.*, 1999). The fault-bounded tectonic subsidence caused 4km long section of the coast near Golcuk to submerge about 2 to 3m, with considerable

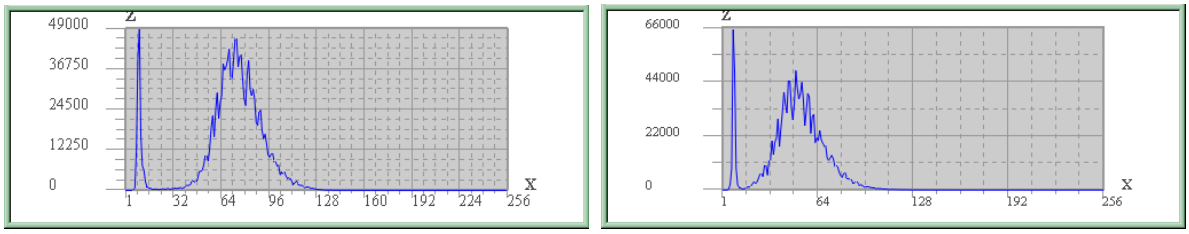

(a) Pre-event. (b) Post-event.

Figure 4.1.4. Histogram of the near infrared band.

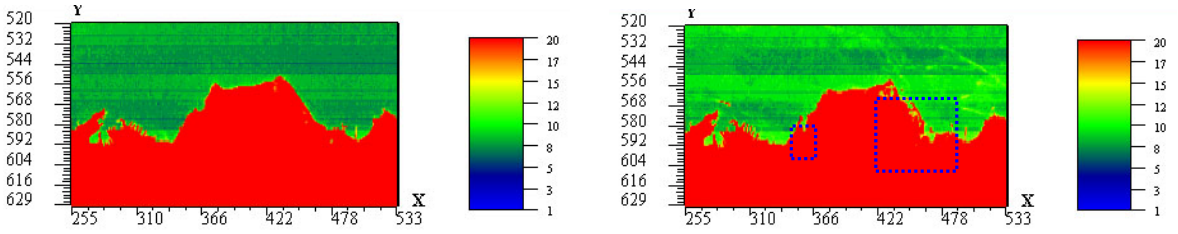

(a) Pre-event image. (b) Post-event image.

Figure 4.1.5. The difference in the sunken area is highlighted by matching the pre- and post-event images (Refer to color Figure 7).

flooding of buildings and loss of lives by drowning.

The characteristic spectral reflectance curve for water bodies shows a general reduction in reflectance with increasing wavelength, so that in the near infrared the reflectance of deep, clear water is virtually zero. To detect those areas sunk into the Sea of Marmara we have used the near infrared band (band 4). The histograms of the images are matched so that we obtain an apparent distribution of the brightness values in certain range, and as a result we obtain two images in which the differences of water bodies are highlighted. The histograms of the pre- and post-event images that correspond to the near infrared band of the region of interest (see Figure 4.1.1) are shown in Figure 4.1.4. In these graphs it can be seen that the histogram has two sectors, which the left part represents the distribution of the water's reflectance. Since the reflectance value of the water in the near infrared band is low, we match the histograms in the range 1 to 20 and obtain the images in Figure 4.1.5. Comparing these two images, it can be seen that in the image of the post-event (Figure 4.1.5(b)) there are some areas that differ from those in the pre-event image. These differences represent the inundated areas.

4.1.4 Building Damage

Ratios between images are effective in enhancing or reveling information when there is an inverse relationship between two spectral responses to the same physical phenomena (Campbell, 1996). If two spectral responses have the same spectral behavior, the ratio provides little additional information. But if they have quite different spectral responses, the ratio between two values provides a single value that concisely expresses the contrast between the reflectance from two images. In this study two kind of ratios have been studied, the Infrared/Red ratio and the Normalized Difference Vegetation Index (*NDVI*). The second index gave better results that are presented in this study. The *NDVI* is defined as follows:

$$NDVI = IR - R / IR + R \tag{4.1}$$

Since our data comes from Landsat/TM satellite the *IR* and *R* bands correspond to band 4 and band 3, respectively. As a result of the arithmetic operations we have obtained two enhanced images (Figure 4.1.6) that correspond to the images before and after the earthquake.

In the center of the image (b) of Figure 4.1.6 a bright area can be distinguished that highly differs from the corresponding area in the pre-event image. Within this area there are damaged buildings at different levels, from slightly damage to total collapse. The brightness in this area is due to the spread of debris after the building collapse.

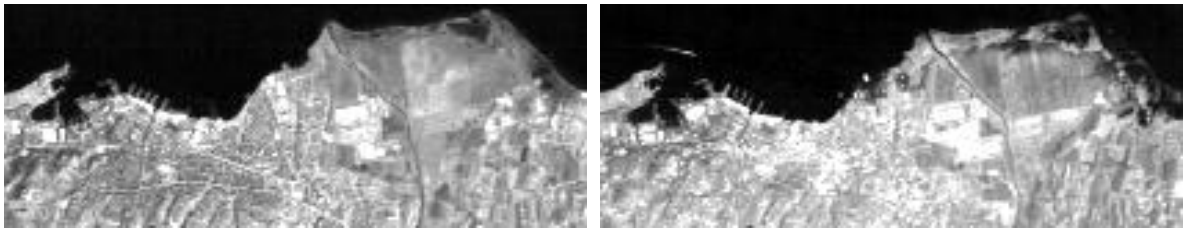

(a) Pre-event image. (b) Post-event image.

Figure 4.1.6. Images obtained through Normalized Difference Vegetation Index (*NDVI*) (Refer to color Figure 8).

4.1.5 Comparison with Ground Truth Data in Golcuk

A detailed and systematic field survey on building damage was conducted by a Japanese team in Golcuk and Degirmendere (AIJ Reconnaissance Team, 1999). Using the survey data, the damage ratios of buildings in the city-block level were calculated. Figure 4.1.7 shows the collapse ratio of the buildings evaluated for each block in Golcuk, defined as the ratio of the number of buildings classified as collapsed and the total number of buildings in each block. The ratio of the images, obtained by the *NDVI*, is compared with the ground truth data, for the different levels of damage. To compute the ratio we consider the mean value of the digital numbers that correspond to a region of certain level of damage. This ratio, shown in the Figure 4.1.8, presents a trend from higher values to lowers ones, it means from high to lower reflectance, except for the submerged zones (JGS, 2000), where the ratio is out of this trend.

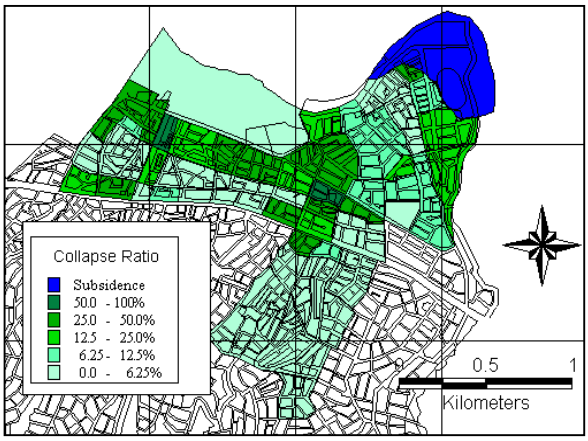

Figure 4.1.7. Distribution of damage in Golcuk by field survey of AIJ and JGS.

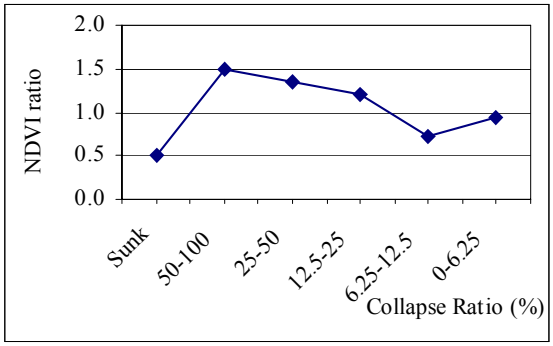

Figure 4.1.8. Ratio of the NDVI: after/before.

4.1.6 Summary

Landsat images before and after the Kocaeli earthquake were investigated. The analyzed region of interest showed different types of damage (i.e., fire, subsidence and various levels of building damage). The analysis of the near infrared band (band 4 in case of Landsat/TM 5 satellite) gives a good approach to detect the flooding. The ratio of the *NDVI* of the images before and after the earthquake gives some trend that conveys some relationship between the different levels of damage. Although the results are in good agreement with the field survey, there is still a high variability in these indexes and a further study using other bands and data from other areas is recommended.

4.2 Interferometric Satellite SAR for Damage Detection

4.2.1 Microwave Scattering in the Areas of Building Damage

According to our previous studies (Aoki *et al*., 1998; Matsuoka and Yamazaki, 2000a), artificial structures show comparatively high reflection due to specular characteristics of structures and ground. Open spaces or damaged buildings have comparatively low reflectance because microwaves are scattered to different directions. A schematic diagram of a surface object and its backscattering property are shown in Figure 4.2.1. Buildings may be reduced to debris by an earthquake, and in some cases, the debris of the buildings may be cleared leaving the ground exposed. Thus, the backscattered intensity determined after a damaging earthquake may become low compared with that obtained before the event. The complex coherence derived from an interferometric analysis is also a suitable and sensitive parameter for detecting superficial changes. Because collapsed buildings exert an influence on phase, the degree of coherence becomes small between pre- and post-event images.

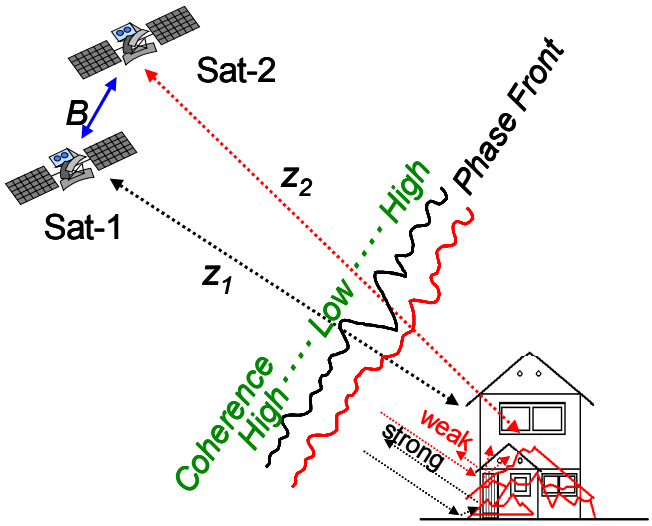

Figure 4.2.1. Schematic diagram for detecting building damage using repeat-pass radar observations.

4.2.2 ERS/SAR Images and Processing

Series of radar observations including tandem flights using ERS-1 and ERS-2 was conducted over the affected area before and after the earthquake. The image pair, which consists of August 13 and September 17, 1999 (pair 8/13-9/17), with 34-day difference and 80m-baseline distance, and the pair of August 12 and August 13, 1999 (pair 8/12-8/13), with 1-day difference and 240m-baseline distance, were used to investigate the variation of backscattering property in the damaged areas. All the images were registered to the 1999/08/13 data by the nearest neighbor method, using tie points derived from the optimum pixel pair determination, by searching pixel by pixel, at the position that yields the highest correlation between two single-look amplitude images.

Figure 4.2.2 shows a pseudo multi-look amplitude image created by averaging 5 azimuths and one range pixels to single-look one, which observed northwestern region of Turkey on September 17, 1999. The zoom-up image of Golcuk is shown in Figure 4.2.3(a). The amplitude difference value was calculated for each pair, and then the intensity difference images were generated. The image for the pair 8/13-9/17 is shown in Figure 4.2.3(b). The correlation coefficient between two single-look amplitude images was calculated within a small

corresponding window, with pixel sizes of 15 for the azimuth and 3 for the range direction. Following this procedure, we created the correlation images that have the same size as described using a spatial averaging. The correlation image from the pair 8/13-9/17 is shown in Figure 4.2.3(c). The degree of coherence, which indicates the correlation between two co-registered complex SAR images by calculating the phase of the backscattering echo, was also used as an index to indicate the changes in the affected area. The window sizes for the coherence calculation and the averaging were same as those for the intensity correlation calculation. The image for the pair 8/13-9/17 is shown in Figure 4.2.3(d).

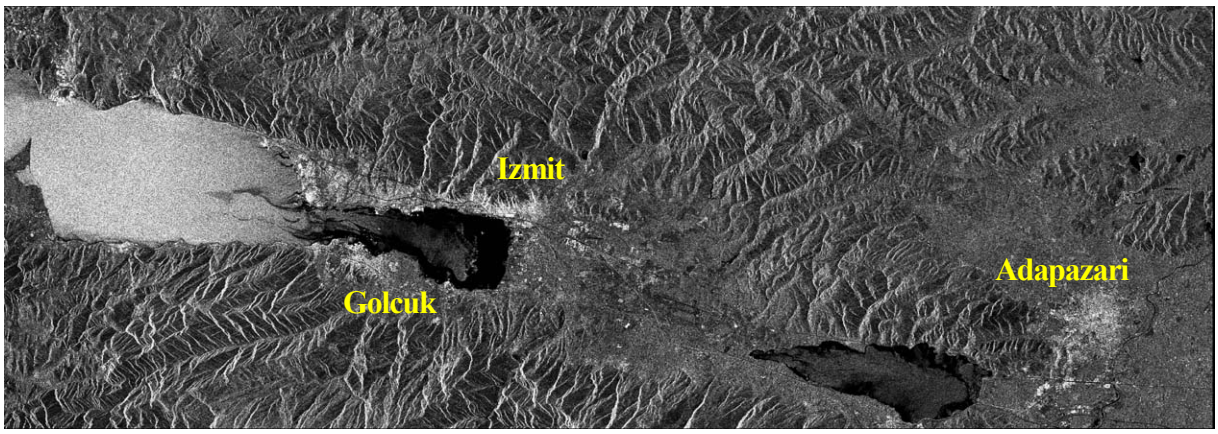

Figure 4.2.2. ERS/SAR amplitude image of northwestern region of Turkey (September 17, 1999; Refer to color Figure 9).

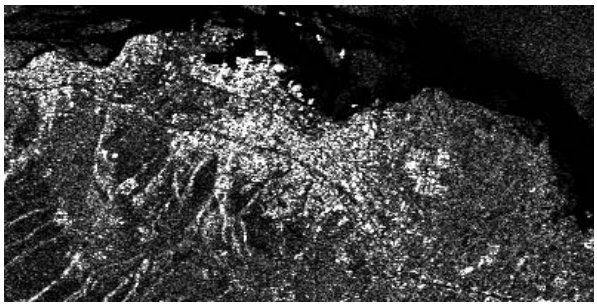

(a) Intensity image (September 17, 1999).

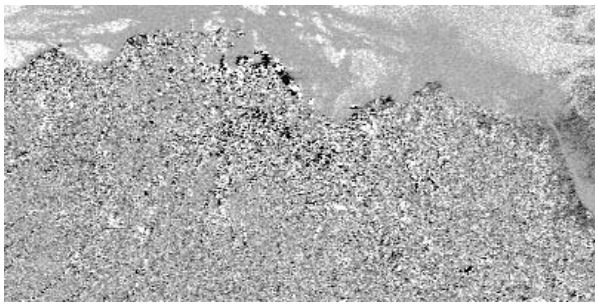

(b) Intensity difference image for the pair 8/13-9/17.

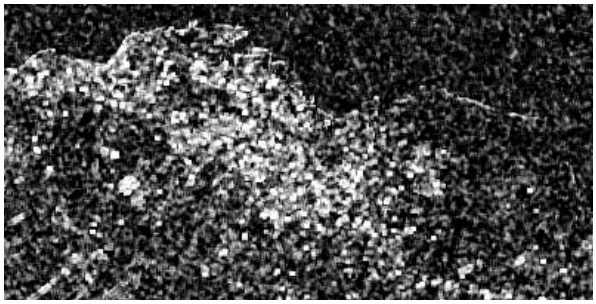

(c) Intensity correlation image for the pair 8/13-9/17.

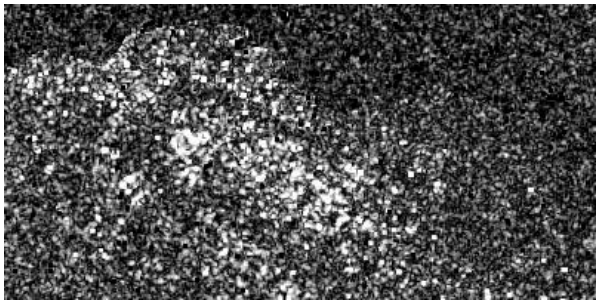

(d) Coherence image for the 8/13-9/17.

Figure 4.2.3. ERS/SAR image of Golcuk.

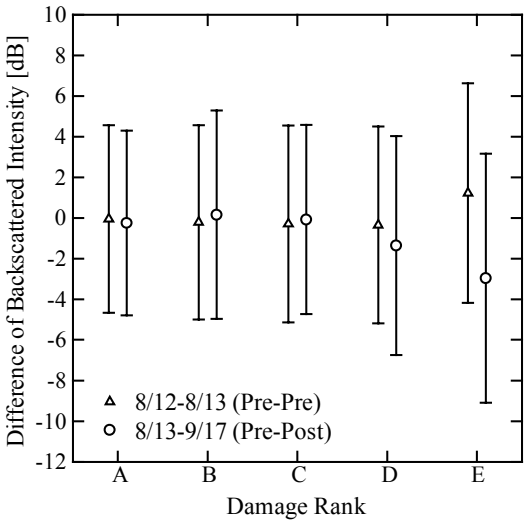

Figure 4.2.4. Difference in backscattered intensities from two time instants for different damage rank.

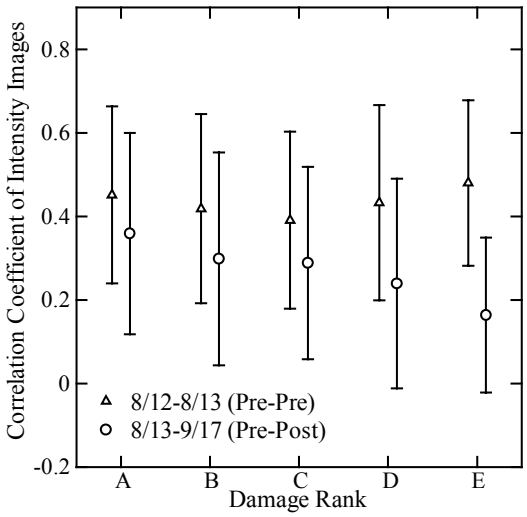

Figure 4.2.5. Correlation coefficient of intensity images between two time instants for different damage rank.

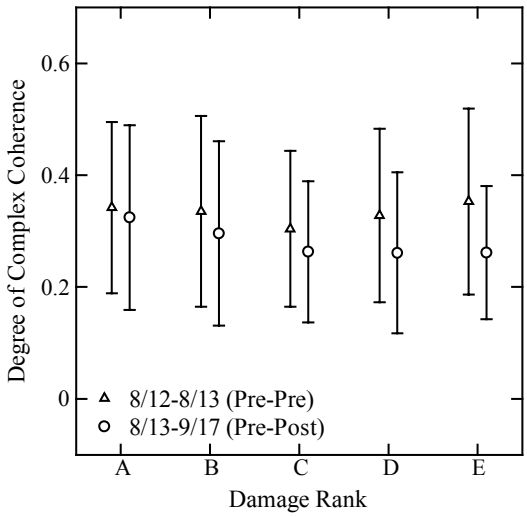

Figure 4.2.6. Degree of complex coherence between two time instants for different damage rank.

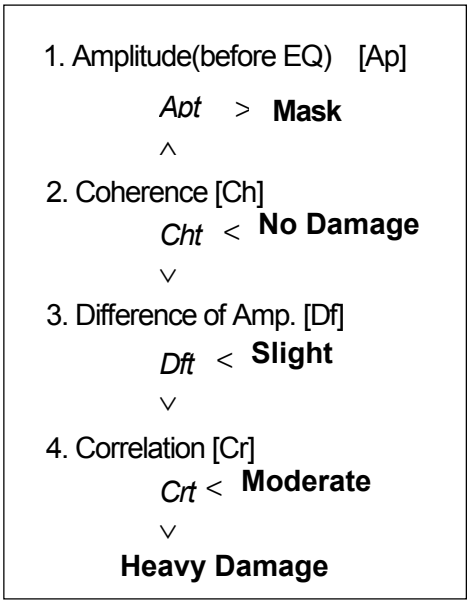

Figure 4.2.7. Procedure for damage estimation.

4.2.3 Backscattering Characteristics of Damaged Areas

The pixels that correspond to the area of each damage rank were selected from the SAR images in order to examine the characteristics of the intensity difference, the intensity correlation, and the degree of complex coherence in the damaged areas. The damage rank (see Figure 4.1.7) was classified into the five categories as rank A, B, C, D, and E, which correspond to the collapse ratios of 0-6.25, 6.25-12.5, 12.5-25, 25-50, and 50-100%, respectively. The numbers of selected pixels were approximately 1,800, 840, 720, 1,000, and 80 for the damage ranks A, B, C, D, and E, respectively.

The characteristics of the mean value and the standard deviation of the intensity difference in each damage

rank for the two pairs are shown in Figure 4.2.4. Although there is a scatter in the intensity difference for each damage rank, the mean value in each rank decreases as the damage rank increases, for the pair 8/13-9/17. This trend is remarkable in the severe damage ratios (D and E). In the pre-event images' pair of 8/12-8/13, this trend cannot be observed because they are not affected by the destruction due to the earthquake.

The same behavior in case of the intensity correlation and the complex coherence are shown in Figures 4.2.5 and 4.3.6, respectively. As the damage level increases the intensity correlation decreases gradually for the pair 8/13-9/17, which agrees with the results of the Kobe study (Matsuoka and Yamazaki, 2000). As shown in Figure 4.2.6, the degrees of coherence in the slight damage area (A) are relatively high in comparison with those in the moderate (B, C) or heavy damaged areas (D, E) for the pair 8/13-9/17 although the standard deviations are quite large. For the pre-event pair 8/12-8/13, the correlation of backscattered intensity and the damage level are seen to have no relationship. A similar tendency for the two pairs is observed in the complex coherence shown in Figure 4.2.6.

4.2.4 Estimation of Damage Distribution

According to the results obtained above, it is found that the intensity difference can identify large surface changes, and that the intensity correlation is sensitive to a wide range of earth surface changes while the degree of coherence is sensitive to only slight surface changes. A simple procedure shown in Figure 4.2.7 can be proposed to extract the damage areas based on a level slice method. We determined and assigned threshold values, *Cht* (value is 0.35), *Dft* (-2.0), and *Crt* (0.2) in the coherence, the amplitude difference, and the correlation images, respectively. First, the pixels whose coherence values are smaller than the *Cht* are assigned as non-damaged. The pixels whose coherence vales are greater than or equal to *Cht* are moved to the next step of the discriminate procedure. Then, slightly damaged areas are extracted using the *Dft* in the difference image. The pixels whose correlation vales are smaller than *Crt* are assigned to heavily damaged. The rest of pixels are assumed to be moderately damaged.

The result of the estimation is shown in Figure 4.2.8. In Golcuk area, the estimated damage distribution from SAR images almost corresponds to the result of the field survey. The heavily damaged and non-damaged areas spread widely in Adapazari and Izmit areas, respectively. These results are relatively good agreement with the several damage survey reports (e.g., AIJ Reconnaissance Team, 1999; MCEER, 2000). However, since

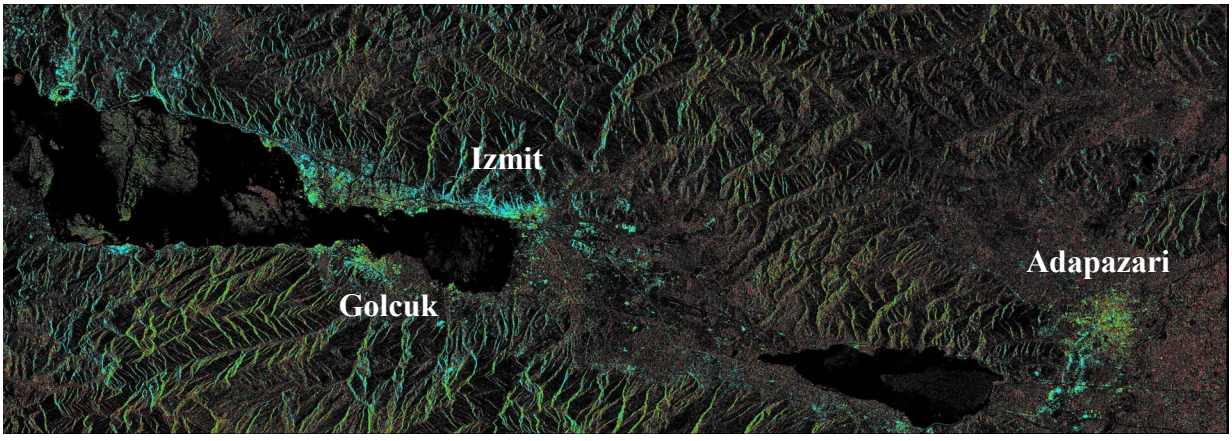

Figure 4.2.8. Estimated damage distribution overlaid on SAR amplitude image
(Heavy: red, Moderate: yellow, Slight: green, No damage: blue; Refer to color Figure 10).

these results were derived from the pairs with short baseline distances and using C-band microwaves, a further study based on SAR images with different acquisitions and satellites should be necessary to reach a general conclusion on grasping damage distribution from the space.

4.2.5 Summary

This section demonstrated a quantitative evaluation on the backscattering properties of SAR images, such as the difference of intensities, intensity correlation, and complex coherence between different acquisitions for the areas hit by the 1999 Kocaeli earthquake. ERS/SAR images taken before and after the event and detailed field survey data were employed to examine the possibility of capturing the damage distribution. The building damage ratio for city blocks obtained by the field survey and the backscattering properties derived from the SAR images were compared.

In the areas of heavy building damage, the backscattered intensity and the intensity correlation between the pre- and post-event images were found to become low. The degree of complex coherence was found to be useful to classify small damage levels. The estimated damage distribution from the SAR images almost corresponded to the results by a field survey. In spite of these results regarding the mean characteristics of the SAR images, a large degree of randomness exists in the backscattering properties for each damage classification. A further study is suggested till a general statement for the earthquake damage survey in urban areas using satellite SAR is made.

Acknowledgements

The Landsat/TM and ERS/SAR images used in this study were provided by European Space Agency under a cooperative research agreement established for this earthquake.

References

AIJ Reconnaissance Team (Kabeyasawa, T. *et al.*) (1999). "Progress report on damage investigation after Kocaeli earthquake by Architectural Institute of Japan," *Proc. ITU-IAHS International Conference on the Kocaeli Earthquake 17 August 1999*, Istanbul Technical University, Istanbul, Turkey, pp. 239-270.

Aoki, H., Matsuoka, M., and Yamazaki, F. (1998). "Characteristics of satellite SAR images in the damaged areas due to the Hyogoken-Nanbu Earthquake," *Proc. 19th Asian Conference of Remote Sensing*, pp. C7/1-6.

Aydan, O. (1999). "The 1999 Kocaeli Earthquake, Turkey -Investigation into damage to civil engineering structures," *Earthquake Engineering Committee*, Japan Society of Civil Engineers, pp. 12.1-12.13.

Campbell, J. B. (1996). *Introduction to Remote Sensing –Second Edition*, Taylor & Francis, London.

Estrada, M., Matsuoka, M., and Yamazaki, F. (2000b). "Use of optical satellite images for the recognition of areas damaged by earthquakes," *Proc. the 6th International Conference on Seismic Zonation* (to appear).

Matsuoka, M. and Yamazaki, F. (1998). "Identification of damaged areas due to the 1995 Hyogoken-Nanbu Earthquake using satellite optical images," *Proc. 19th Asian Conference of Remote Sensing*, pp. Q9/1-6.

Matsuoka, M. and Yamazaki, F. (2000a). "Interferometric characterization of areas damaged by the 1995 Kobe Earthquake using satellite SAR images," *Proc. 12th World Conference on Earthquake Engineering*, CD-ROM, Paper ID 2141.

Matsuoka, M. and Yamazaki, F. (2000b). "Use of interferometric satellite SAR for earthquake damage detection," *Proc. the 6th International Conference on Seismic Zonation* (to appear).

Multidisciplinary Center for Earthquake Engineering Research (2000). *The Marmara, Turkey Earthquake of August 17, 1999: Reconnaissance Report*, MCEER-00-0001.

Rosen, P. A., Hensley, S., Peltzer, G., Rignot, E., and Werner, C. (1999). "JERS-1 synthetic aperture radar interferometry applications, - Mapping of rain forest environment and crustal deformation studies," *JERS-1 Science Program '99 PI Reports, Global Forest Monitoring and SAR Interferometry*, Earth Observation Research Center, NASDA, pp. 179-184.

The Japanese Geotechnical Society (2000). "Report on the investigations of the 1999 Kocaeli earthquake, Turkey," CD-ROM (in Japanese).

Yonezawa, C. and Takeuchi, S. (1998). "Detection of damaged built-up areas by the 1995 Hyogoken-Nanbu Earthquake using ERS-1/SAR intensity images," *Photogrammetric Engineering and Remote Sensing*, Vol. 37, No. 4, pp. 57-61 (in Japanese).

Yonezawa, C. and Takeuchi, S. (1999). "Detection of urban damage using interferometric SAR decorrelation," *Proc. International Geoscience and Remote Sensing Symposium*, IEEE, CD-ROM.